Scientia Iranica A (2017) 24(5), 2183–2201

Sharif University of Technology
Scientia Iranica
Transactions A: Civil Engineering
www.scientiairanica.com

Attenuation relation for near-field shallow crustal earthquakes using NGA-West2 database with mixed-effect model in comparison with attenuation relations for Iran

A. Shokran Neam and T. Taghikhany*

Department of Civil and Environmental Engineering, Amirkabir University of Technology, Tehran, Iran.

Received 24 August 2014; received in revised form 26 December 2015; accepted 25 July 2016

KEYWORDS
Empirical attenuation relationship;
NGA;
Mixed effects model;
Nonlinear model;
Iran plateau.

Abstract. This study presents a new empirical equation for the estimation of horizontal strong ground motions caused by shallow crustal earthquakes. This model was developed empirically by regression of the database, which was used by the NGA-West2 GMPE developers with a fault rupture distance less than 60 kilometers. The data set consisted of corrected and processed accelerograms of 1545 strong-motion records of earthquakes between 5.2 and 7.9 M_w. The model was a function of earthquake magnitude, distance of source from site, local average shear wave velocity, nonlinear soil response, sediment depth, rupture dip, faulting mechanism, and hanging wall effect. This equation was derived by a stable algorithm for regression analysis called mixed effect model. The algorithm was used to develop PGA and PSA (T_1) for periods from 0.01 to 10.0 seconds. Major differences between this model and the recently developed attenuation relations for the world and Iran were observed for large-magnitude ground motions, which were recorded at small-to-moderate distances from seismic source. The results showed that the near-field affected the predicted values, especially in soil sites. Moreover, comparison with the attenuation relations developed by Iranian data set confirmed that the equation in this region was sensitive more to distance than to other parameters.

1. Introduction

One of the important steps in the process of seismic structural design is selecting an appropriate site-specific ground motion. This stage is highly dependent on the earthquake source characterizing parameters, the propagation path, and geological conditions. Distinguishing the effect of these parameters on ground motion is rather complicated. In seismic hazard analysis, the effects of these aspects are estimated by empirical attenuation relationships. The equation which is employed for prediction of ground motion (attenuation relationship) is a mathematical equation (i.e. a model) that relates a given strong-motion parameter to one or more parameters of the earthquake source, wave propagation path, and local site. The design of ground motions is often controlled by hypothesized occurrence of a large earthquake on nearby faults; therefore, it is important that the seismological models or attenuation relationships properly estimate ground motions at near-filed. In recent decades, several near-field attenuation equations have been provided for es-

*. *Corresponding author.*
E-mail addresses: shokran@aut.ac.ir (A. Shokran Neam); ttaghikhany@aut.ac.ir (T. Taghikhany)

doi: 10.24200/sci.2017.4152

timating ground motions at short distance of causative fault [1,2] by increasing the number of recorded ground motions at close distance of causative faults.

The Pacific Earthquake Engineering Research center (PEER) initiated a project in 2003 to develop the next generation attenuation relationships (called NGA-West1). The developed Ground Motion Prediction Equations (GMPEs) are widely used in seismology and engineering [3-6] attempting to render a more realistic model by utilizing a different regression method, adding new parameters, and considering near-field effects. In 2013, the NGA-West2 research project, which was the second phase of NGA-West1, addressed additional and complementary ground motion issues. Thousands of ground motions recorded worldwide since 2003 were processed and added to the NGA database. The size of the NGA-West2 database was twice that of NGA-West1 [7].

The equation presented in the current study is developed empirically by regression of the database, which is used by the NGA-West2 GMPE developers with fault rupture distance of less than 60 km. This attenuation relation predicts the average horizontal acceleration response spectra component of shallow crustal near-field regions.

Herein, the specific numerical optimization method is applied based on Genetic Algorithms (GA) for solving the numerical equation of mixed effect to determine the optimum values of the design variables while reducing the error to an acceptable value. Next, seismological and geotechnical information and a set of strong motion recordings with new constraints imposed on the earthquake parameters and refined functional forms are used to develop a mutually consistent set of strong ground motion relations for the average horizontal components of Peak Ground Acceleration (PGA) and 5% damped Pseudo Spectral Acceleration (PSA(T_1)). This equation comprises the recently developed functions for simulating the effect of different parameters on ground motion for yielding more accurate estimates. Further, by eliminating the uncertain records, the employed data becomes more uniform and, thus, unrealistic estimates are avoided.

Lastly, so as to investigate the consistency of the introduced equation with Iranian plateau, it has been compared with the descript attenuation relation, which was extended for Iran for the period 1999 to 2010.

2. Strong motion data

The database used for this study was a subset of the PEER strong motion database, which was downloaded from the PEER website at http://peer.berkeley.edu/nga/index.html. In this regard, 1545 strong motion records were selected from 79 shallow crustal earthquakes between 1940 and 2011. All data were free-field records (recordings from buildings of less than three stories, or less than seven stories if located on a firm rock). Further limitations were considered for data selection in this study due to engineering requirements and seismological issues. In order to have near-field specific attenuation equation, the data set was selected from records with rupture distance less than 60 km. Better correlation can be observed between magnitude and distance at short distance of causative fault since inelastic decay of the seismic wave propagation is negligible [8].

It is worth to note that the records with larger source-to-site distances were excluded due to their low engineering significance [9], and to avoid records with several reflections from lower layers that happened during some earthquakes, although some authors believe that ground motion prediction is valid for distances of less than 300 km, where $R_{\text{rup}} \leq 60$ km would include the major part of strong ground motion investigation of engineering seismology [8].

The data set was selected from earthquakes with Moment Magnitudes (M_w) more than 5.2, since an earthquake of less than this magnitude did not control the structural performance at short distance of earthquake source. The focal depth (h) of selected records was limited to 20 km as the scope of the present study was limited to the shallow crustal ground motions [8].

In order to enhance quality of the database, the records on the toe or base of a dam were excluded because of the potential adverse effects of instrument embedment and soil-structure interaction [4]. Moreover, the data from subduction zones were excluded due to the differences of tectonic regimes and shallow crustal earthquakes [8].

In addition to the above criteria, the records with the following characteristics were excluded from the database [8]:

1. The records of the earthquakes which did not have sufficient records;
2. The records which had only one horizontal or vertical component;
3. Recordings without v_{s30} estimate (v_{s30}: the average shear-wave velocity in the top 30 m of a soil profile);
4. The records of the earthquakes which lacked key source data;
5. The records which exhibited strong topographic effects (recordings from the Tarzana Cedar Hill Nursery);
6. An aftershock occurred in the immediate vicinity of the inferred main-shock rupture plane, which has been considered by authors potentially below-average stress, drops however, this will not happen to events "triggered" by the main shock (e.g., the

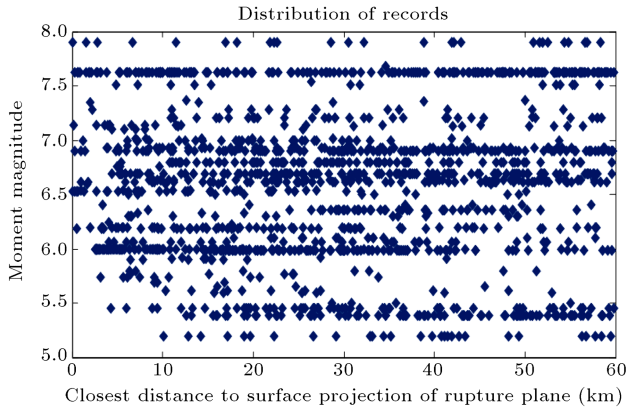

Figure 1. Distribution of record dataset with respect to magnitude and distance.

1992 Big Bear earthquake), which is considered to have a similar stress regime as the main shock [6].

Table 1 lists the selected records and their characteristics. Despite the fact that the effect of tectonic environment on strong ground motions has been known in recent years, because of the limited number of records, this effect is not recognized in the database utilized in the present study [10].

Figure 1 shows the distribution of the data with their magnitude and distance: $5.2 \leq M_w \leq 7.9$ and $0 \leq R_{\text{rup}} \leq 60$ (km). Data were well distributed in magnitude-distance space, suggesting that there was no need to use special statistical procedures to decouple source and path effects in the regression analysis. Peak Ground Acceleration (PGA) and 5% damped Pseudo Spectral Acceleration (PSA (T_1)) at natural periods ranging from 0.01 to 10.0 seconds were used as strong motion parameters.

Faulting mechanisms of the selected earthquakes in the dataset were classified into four categories, namely, strike slip, normal, oblique, and reverse. Due to fault segmentation, there was a lack of recordings with normal mechanisms in the dataset for earthquakes with $M_w > 6.9$. Different studies show that earthquakes with normal faulting mechanisms at some certain periods and distances have lower median of predicted ground motion in extensional stress environments than in compressional stress fields Spudich and Joyner [10,11].

3. Mixed effects model for regression analysis

The fixed effects regression model, which is the usual approach for deriving empirical attenuation relations, is defined as follows [12]:

$$\ln y_{ij} = f(P_{ij}, \theta) + \varepsilon_{ij}, \tag{1}$$

where y_{ij} is the ground motion intensity parameter, $f(P_{ij}, \theta)$ denotes the ground-motion prediction function with predictive parameters, P_{ij} (e.g., magnitude, distance of source from site, site condition) and coefficient set θ, and ε_{ij} is the error term for the jth recording from the ith event and is assumed to be normally distributed with mean zero. This model is used for estimation of all dependencies that are taken into consideration.

Another regression method is mixed effects model, which includes both fixed effects and random effects [12]. The random or variance component effect is the maximum likelihood of dependencies between data items that are subjected to implicit estimation. For example, if an earthquake has a stress drop higher than average, then the ground motion at all sites from this event is expected to be higher than average. However, if seismologists want to compare the event terms so as to better understand the ground motions, then the event terms should be treated as fixed effects.

For the mixed effects model, the error term is partitioned into two parts: inter-event and intra-event terms. The regression model is formulated as follows:

$$\ln y_{ij} = f(P_{ij}, \theta) + \eta_i + \varepsilon_{ij}, \tag{2}$$

where η_i and ε_{ij} represent inter-event and intra-event variations, respectively, and are assumed to be independent and normally distributed random parameters. The maximum likelihood method [13] is used to partition the residual for each recording into η_i and ε_{ij}. In this method, the expectation-maximization algorithm is used for computing the model parameters (θ) and variances of η_i and ε_{ij} (σ^2 and τ^2). The algorithm is an iterative procedure in which the random effects, variances, and model parameter values are computed successively.

For normally distributed data, the likelihood is given by:

$$\begin{aligned}\ln L = &-\left(\frac{1}{2}\right) N \ln(2\pi) - \left(\frac{1}{2}\right)(N-M)\ln\sigma^2 \\ &-\left(\frac{1}{2}\right)\sum_{i=1}^{M}\ln\left(\sigma^2 + n_i\tau^2\right) \\ &-\left(\frac{1}{2\sigma^2}\right)\sum_{i=1}^{M}\sum_{j=1}^{n_i}(y_{ij}-Y_i)^2 \\ &-\left(\frac{1}{2}\right)\sum_{i=1}^{M}\Big(n_i(Y_i-\mu_i)/(\sigma^2+n_i\tau^2)\Big),\end{aligned} \tag{3}$$

$$Y_i = \left(\frac{1}{n_i}\right)\sum_{j=1}^{n_i} y_{ij}, \tag{4}$$

$$\mu_i = \left(\frac{1}{n_i}\right)\sum_{j=1}^{n_i} \mu_{ij}, \tag{5}$$

Table 1. Database of strong-motion recordings.

Number of records	Mechanism based on rake angle	Earthquake magnitude (M_w)	Year	Location	Earthquake name
1	Strike slip	6.95	1940	Western United States (WUS)	Imperial Valley
1	Thrust	7.36	1952	WUS	Kern County
4	Strike slip	6.19	1966	WUS	Parkfield
1	Strike slip	6.63	1968	WUS	Borrego Mtn
19	Thrust	6.61	1971	WUS	San Fernando
1	Strike slip	7.68	1972	Alaska	Sitka
1	Strike slip	6.24	1972	Nicaragua	Managua
1	Reverse oblique	7.21	1976	Turkey	Caldiran
1	Reverse	6.80	1976	USSR	Gazli
3	Thrust	6.50	1976	Italy	Friuli-1
4	Thrust	5.91	1976	Italy	Friuli-2
3	Thrust	7.35	1978	Iran	Tabas
2	Thrust	5.92	1978	WUS	Santa Barbara
4	Strike slip	6.00	1978	Italy	Basso Tirreno
1	Thrust	7.54	1979	Alaska	St Elias
33	Strike slip	6.53	1979	WUS	Imperial Valley-6
10	Strike slip	5.74	1979	WUS	Coyote Lake
5	Reverse	7.10	1979	Yugo	Montenegro
12	Normal	6.90	1980	Italy	Irpinia-1
9	Normal	6.20	1980	Italy	Irpinia-2
4	Strike slip	6.33	1980	Mexico	Victoria, Mexico
3	Reverse oblique	6.06	1980	WUS	Mammoth Lakes-1
3	Strike slip	5.69	1980	WUS	Mammoth Lakes-2
1	Normal	6.60	1981	Greece	Corinth
6	Strike slip	5.90	1981	WUS	Westmorland
46	Thrust	6.36	1983	WUS	Coalinga
26	Strike slip	6.19	1984	WUS	Morgan Hill
5	Normal	5.80	1984	Italy	Lazio-Abruzzo
6	Normal	5.6	1984	Italy	Umbria-03
3	Thrust	6.76	1985	Canada	Nahanni
1	Reverse oblique	5.20	1985	Greece	Drama
5	Strike slip	6.19	1986	WUS	Chalfant Valley-1
11	Strike slip	5.77	1986	WUS	Chalfant Valley-2
26	Reverse	6.06	1986	WUS	N. Palm Springs
2	Strike slip	5.80	1986	WUS	San Salvador
1	Normal	6.60	1987	New Zealand	New Zealand
1	Strike slip	6.22	1987	WUS	Superstition Hills-1
11	Strike slip	6.54	1987	WUS	Superstition Hills-2
107	Reverse	5.99	1987	WUS	Whittier Narrows-1
57	Reverse	6.93	1989	WUS	Loma Prieta
2	Strike slip	7.37	1990	Iran	Manjil
2	Normal	6.10	1990	Greece	Griva
9	Thrust	5.61	1991	WUS	Sierra Madre

Table 1. Database of strong-motion recordings (continued).

Number of records	Mechanism based on rake angle	Earthquake magnitude (M_w)	Year	Location	Earthquake name
13	Strike slip	7.28	1992	WUS	Landers
6	Thrust	7.01	1992	WUS	Cape Mendocino
1	Strike Slip	6.69	1992	Turkey	Erzican
3	Normal	5.65	1992	WUS	Little Skull Mtn
5	Strike slip	6.10	1992	CA	Joshua Tree
1	Strike slip	5.90	1994	WUS	Double Springs
128	Thrust	6.69	1994	WUS	Northridge
1	Strike slip	7.20	1995	WUS	Gulf of Aqaba
7	Strike slip	6.90	1995	Japan	Kobe
3	Normal	6.40	1995	Turkey	Dinar
3	Normal	6.40	1995	Greece	Kozani
8	Normal	6	1997	Italy	Umbria Marche
4	Normal	5.2	1997	Italy	Umbria Marche-8
8	Strike slip	7.13	1999	WUS	Hector Mine
15	Strike slip	7.14	1999	Turkey	Duzce
13	Strike slip	7.51	1999	Turkey	Kocaeli
209	Reverse oblique	7.62	1999	Taiwan	Chi-Chi
42	Strike slip	6.61	2000	Japan	Tottori
4	Strike slip	7.90	2002	Alaska	Denali
6	Reverse	6.5	2003	CA	San Simeon
2	Strike slip	6.6	2003	Iran	Bam
76	Strike slip	6.00	2004	CA	Parkfield-02
40	Reverse	6.63	2004	Japan	Niigata
18	Strike slip	5.20	2005	—	14151344
88	Reverse	6.80	2007	Oki	Chuetsu
60	Strike slip	5.45	2007	—	40204628
86	Reverse oblique	5.39	2008	—	14383980
99	Reverse	6.90	2008	Japan	Iwate
22	Reverse oblique	7.90	2008	China	Wenchuan
6	Strike slip	6.10	2008	China	Wenchuan-02
4	Strike slip	5.50	2008	China	Wenchuan-09
5	Reverse	5.20	2008	China	Wenchuan-38
13	Normal	6.30	2009	Italy	L'Aquila
31	Strike slip	7.20	2010	Cucapah	El Mayor
32	Strike slip	7.00	2010	New Zealand	Darfield
29	Reverse oblique	6.20	2011	New Zealand	Christchurch

where N is the number of records, n_i is the number of records in the ith earthquake, M is the number of earthquakes, and μ_{ij} is the predicted value:

$$\mu_{ij} = f(P_{ij}, \theta).$$

σ and τ are estimated to maximize the likelihood function (Eq. (3)) by numerical optimizations (genetic algorithm, as employed in this research). Now, for a given θ and the maximum likelihood estimates of σ and τ, the random-effects term, η_i, is estimated as follows:

$$\eta_i = \tau^2 \sum_{j=1}^{n_i} (y_{ij} - \mu_{ij})/n_i\tau^2 + \sigma^2. \quad (6)$$

When an earthquake has just a single recording, the percentage of the residuals that are assigned to the inter-event term can be obtained by the ratio $\tau^2/\tau^2 + \sigma^2$. On the other hand, if there is a large number of recordings from an earthquake, then the inter-event term becomes the mean residual for that event. Thus, the maximum likelihood model partitions the error in a meaningful way [14].

Estimated value of η_i results in a new set of coefficients, θ, in comparison with only fixed effects model ($\ln(Y_{ij}) - \eta_i = f(P_{ij}, \theta) + \varepsilon_{ij}$). The new set θ is then used to re-estimate σ, τ, and η, and this iterative algorithm is continued until the coefficients converge on specific values.

In summary, the steps of the mixed effects algorithm are presented as follows [8]:

1. Estimate the model coefficients θ using a fixed effects regression algorithm assuming η equal to 0;
2. Use θ for solving the variances of the residuals, σ^2 and τ^2, by maximizing the likelihood function described in Eq. (3);
3. Given θ, σ^2, and τ^2, estimate η_i using Eq. (6);
4. Given η_i, estimate the new coefficients (θ) using a fixed effects regression algorithm for $\ln(y_{ij}) - \eta_i$;
5. Repeat steps 2-4 until the likelihood in step 2 is maximized and the estimates for the set of coefficients converge.

This algorithm typically converges in less than 30 iterations. The total aleatory standard deviation of the geometric mean is given by the following equation:

$$\sigma_{\text{total}} = \sqrt{\sigma^2 + \tau^2}. \tag{7}$$

4. Optimum analysis of maximum likelihood function using Genetic Algorithm (GA)

Genetic Algorithm (GA) is an optimization tool to minimize an objective function. It is based on the idea that the production of natural processes is optimum and the method of reproduction in natural evolution is optimum itself. First, the collection of feasible solutions (chromosomes) is considered in GA and, then, better solutions are selected using sampling methods. If the selected chromosomes are not the chromosomes with the best fitness function, the same processes governing natural systems, such as mutation and crossover (recombination), are applied to the selected answers. Thus, a new collection of solutions will be generated as a new generation. This process is iterated to reach more progressed generations with the best mean fitness. At the end, the chromosomes of the generations with maximum fitness to the problem will be selected as the optimum solution [8].

The purpose of using Genetic Algorithm in this research is to solve function (3) to find the optimum variances of the residuals. Further, this method does not depend on the initial value of the variables and obtains variances with maximum fitness to the function. For calculation of function (3), most of the settings in the algorithm are based on the default settings in Matlab program, which are listed in Table 2 [8].

Table 2. Settings in genetic algorithm for optimum analysis of maximum likelihood function.

General setting	Fitness function	Eq. (3)					
	Number of variables	2 (σ, τ)					
	Constraints	$0 \leq \tau, \sigma \leq 1$					
	Population type	Double vector					
	Population size	20					
	Creation function	Initial range					
	Selection function	stochastic uniform					
Genetic operators	Reproduction	**Elite count**			**Crossover fraction**		
		2			0.8		
	Mutation function	Use constraint dependent default					
	Crossover function	Scattered					
	Migration	**Interval**		**Fraction**		**Direction**	
		20		0.2		Forward	
General setting	Algorithm setting	**Penalty factor**			**Initial penalty**		
		100			10		
	Stopping criteria	**Function tolerance**	**Stall time limit**	**Stall generations**	**Fitness limit**	**Time limit**	**Generations**
		1e-6	Inf	50	- Inf	Inf	100

5. Median ground motion model

The equation which has been selected to represent median ground motion relations in this study for both the average horizontal components of PGA and PSA (T_1) is given by:

$$\ln Y = f_{\text{mag}} + f_{\text{mag,dis}} + f_{\text{flt}} + f_{\text{site}} + f_{\text{sed}} + f_{\text{hng}} + f_{Z\text{top}} + f_{\text{dip}}. \quad (8)$$

5.1. Scaling of magnitude (f_{mag})

A polynomial function, rather than linear function, is used in this part to model the saturation phenomenon in magnitude scaling at short distance. Due to this effect, the observed magnitudes in stations at short distance of seismic source are less than the real values. The scaling of magnitude term is given by Abrahamson and Silva [5]:

$$f_{\text{mag}} = a_1(T) + a_2(T)(M_w - c) + a_4(T)(8.5 - M_w)^2, \quad M_w \le c, \quad (9.1)$$

$$f_{\text{mag}} = a_1(T) + a_3(T)(M_w - c) + a_4(T)(8.5 - M_w)^2, \quad M_w > c, \quad (9.2)$$

where M_w is moment magnitude, and c is constant factor of 6.5.

This functional form is not adequate for long periods and higher order terms are required [5,11,14].

5.2. Distance term ($f_{mag,dis}$)

The shortest distance to the rupture plane (R_{rup}) in the model has been selected in compliance with the equation introduced by Abrahamson and Silva [5]. This can be explained by their use of a function which fitted small- and large-magnitude recordings and better fitted the data at short distances. Another advantage of the Abrahamson-Silva functional form over other models is its transitional form in magnitude-dependent attenuation term, which makes the nonlinear regression analysis more stable [6]. The distance term is given by the following equation [5]:

$$f_{\text{mag,dis}} = [a_5(T) + a_6(T)(M_w - c)] \ln \sqrt{R_{\text{rup}}^2 + a_7^2(T)}, \quad (10)$$

where R_{rup} (km) is the distance nearest to the co-seismic rupture plane.

The term $a_6(T)$ is constrained to vary monotonically with period; otherwise, the spectral shape in very short distances will yield a large number of errors due to model extrapolation.

5.3. Style-of-faulting term (f_{flt})

The distinctions between strike slip, reverse, oblique, and normal events in attenuation relations are presented by the style of faulting mechanism. Most attenuation relations have considered a constant style of faulting mechanism applied to all magnitudes, distances, and periods. The oblique fault style term has been included in the equation as a new option in comparison with the currently used attenuation relations. With regard to this, the style of faulting mechanism is given as a period-dependent function [9]:

$$f_{\text{flt}} = a_8(T)FR + a_9(T)FN + a_{10}(T)FO, \quad (11)$$

where:

$FR = 1$ is an indicator variable representing reverse fault;

$FN = 1$ is an indicator variable representing normal fault;

$FO = 1$ is an indicator variable representing reverse and normal-oblique.

If FR, FN, and FO are assigned equal to 0, then the function represents strike slip.

5.4. Site response term (f_{site})

The relations between soil amplification and peak ground acceleration on rock site, which have been introduced by many researchers, show that linear functions are not individually sufficient to properly model site response [15,16].

Accordingly, the site response function is divided into two portions, named linear and nonlinear terms.

The function recommended by Boore and Atkinson [17], which is slight modification of the site amplification given by Choi and Stewart [18], is adopted in this paper. These equations are applicable to $180 \le V_{s30} \le 1300$ m/s and should not be applied for very hard rock sites, i.e. $V_{s30} > 1500$ m/s. The coefficients of the function were purveyed in each period and in accordance with NEHRP site category.

The site amplification equation is as follows:

$$f_{\text{site}} = f_{\text{LIN}} + f_{\text{NL}}, \quad (12)$$

where f_{LIN} and f_{NL} are the linear and nonlinear terms, respectively.

5.4.1. Linear site response

The linear part of the site response amplification, which is a function of $\ln(V_{s30})$, was introduced by Boore and Atkinson [17]. This function has proportional relation with periods of less than 0.5 second; however, there is no strong solidarity between V_{s30} and deeper deposit layers in long-period ranges.

The linear site response is given by the following equation:

$$f_{\text{LIN}} = b_{lin} \ln\left(\frac{V_{s30}}{V_{\text{ref}}}\right), \tag{12.1}$$

where b_{lin} is a period-dependent coefficient and V_{ref} is reference velocity of = 760 m/s that is based on NEHRP B/C boundary site conditions.

5.4.2. Nonlinear site response

The main reasons for using non-linear site response term can be summarized as follows:

- The linear part is insufficient to constrain the complex nonlinear behavior of the softer soils;
- The analytical results do not correlate with linear parameters at large ground motions;
- The residuals plotted against rock PGA clearly exhibit a bias due to the nonlinear behavior of PGA and PSA (T_1) at shorter periods. Because of the relatively small number of recordings, the residuals alone could not be used to determine how this behavior varied with V_{s30}, ground motion amplitude, and oscillator period.

The nonlinear site response is given by the following equations [17]:

$pga4nl \leq l_1$:

$$f_{\text{NL}} = b_{nl} \ln\left(\frac{pga\_low}{0.1}\right), \tag{12.2}$$

$l_1 < pga4nl \leq l_2$:

$$f_{\text{NL}} = b_{nl} \ln\left(\frac{pga\_low}{0.1}\right) + c\left[\ln\left(\frac{pga4nl}{l_1}\right)\right]^2 + d\left[\ln\left(\frac{pga4nl}{l_1}\right)\right]^3, \tag{12.3}$$

$l_2 < pga4nl$:

$$f_{\text{NL}} = b_{nl} \ln\left(\frac{pga4nl}{0.1}\right), \tag{12.4}$$

where l_1(= 0.03 g) and l_2 (= 0.09 g) are the breaking points representing the transient region between linear and nonlinear site responses. pga_low(= 0.06 g) is assigned to transition between linear and nonlinear behaviors and $pga4nl$ is the expected peak acceleration in g on rock for V_{ref} = 760 m/s as predicted by median attenuation relation equation (8) with $f_{\text{site}} = f_{\text{sed}} = f_{\text{hng}} = f_{Z\text{top}} = f_{\text{dip}} = 0$.

The period-dependent and V_{s30}-dependent coefficients b_{nl}, c_1, and d are prescribed based on empirical analysis results with slight modifications presented by Choi and Stewart [18], where the modifications were designed to smooth the predicted soil amplifications. b_{nl} (nonlinear slope) is a function of period and V_{s30} is given by the following equations:

$V_{s30} \leq V_1$:

$$b_{nl} = b_1, \tag{12.5}$$

$V_1 < V_{s30} \leq V_2$:

$$b_{nl} = \frac{(b_1 - b_2)\ln\left(\frac{V_{s30}}{V_2}\right)}{\ln\left(\frac{V_1}{V_2}\right)} + b_2, \tag{12.6}$$

$V_2 < V_{s30} \leq V_{\text{ref}}$:

$$b_{nl} = \frac{b_2 \ln\left(\frac{V_{s30}}{V_{\text{ref}}}\right)}{\ln\left(\frac{V_2}{V_{\text{ref}}}\right)}, \tag{12.7}$$

$V_{\text{ref}} \leq V_{s30}$:

$$b_{nl} = 0.0, \tag{12.8}$$

where V_1 = 180 m/s, V_2 = 300 m/s, V_{ref} = 760 m/s, b_1 and b_2 are period-dependent coefficients and b_{nl} is a function of period. The values of these coefficients for different periods have been listed in Table 3.

The coefficients c_1 and d in Eq. (12.8) are given by:

$$c_1 = \frac{3\Delta y - b_{nl}\Delta x}{\Delta x^2}$$

$$d = -\frac{2\Delta y - b_{nl}\Delta x}{\Delta x^3},$$

$$\Delta x = \ln\left(\frac{l_2}{l_1}\right),$$

$$\Delta y = b_{nl} \ln\left(\frac{l_2}{pga\_low}\right), \tag{12.9}$$

where l_1 = 0.03 g, l_2 = 0.09 g and pga_low = 0.06 g.

5.5. Soil depth effect term (f_{sed})

The studies conducted on soil depth effect revealed the different behavior of shallow and deep sediments during earthquake. Preliminary regression analyses on different soils show that by increasing depth, the long-period motions dominate the records up to the depth

Table 3. Period-dependent site-amplification coefficients.

Period	b_{lin}	b_1	b_2
PGA	–0.360	–0.640	–0.14
0.010	–0.360	–0.640	–0.14
0.020	–0.340	–0.630	–0.12
0.030	–0.330	–0.620	–0.11
0.050	–0.290	–0.640	–0.11
0.075	–0.230	–0.640	–0.11
0.100	–0.250	–0.600	–0.13
0.150	–0.280	–0.530	–0.18
0.200	–0.310	–0.520	–0.19
0.250	–0.390	–0.520	–0.16
0.300	–0.440	–0.520	–0.14
0.400	–0.500	–0.510	–0.10
0.500	–0.600	–0.500	–0.06
0.750	–0.690	–0.47	0.00
1.000	–0.700	–0.440	0.00
1.500	–0.720	–0.400	0.00
2.000	–0.730	–0.380	0.00
3.000	–0.740	–0.340	0.00
4.000	–0.750	–0.310	0.00
5.000	–0.750	–0.291	0.00
7.500	–0.692	–0.247	0.00
10.000	–0.650	–0.215	0.00

of $Z_{2.5} = 1$ km. The same behavior can be observed in sediments with depths of more than 3 km [6,19] These effects are defend as:

1. 3-D basin effects for depths of more than 3 km ($Z_{2.5} > 3.0$ km);
2. Shallow-sediment effects for soil depths less than 1 km ($Z_{2.5} < 1.0$ km).

Campbell and Bozorgnia [6] used $Z_{2.5}$ in their model to represent both shallow ($Z_{2.5} < 1.0$ km) and deep ($Z_{2.5} > 3.0$ km) sediment effects. Their function was developed for oscillator periods longer than 2.0 sec. Their model can be used for shorter periods by extrapolation of coefficients. In order to remove any bias, they included an additional model coefficient ($a_{12}(T)$) in Eq. (13) to adjust the coefficient of the model with empirical observations.

Herein, the soil depth effect term is given by:

$$f_{\text{sed}} = \begin{cases} a_{11}(T)(Z_{2.5} - 1) & Z_{2.5} < 1 \\ 0 & 1 \le Z_{2.5} \le 3 \\ a_{12}(T)ke^{-0.75} \left[1 - e^{-0.25(Z_{2.5}-3)}\right] & Z_{2.5} > 3 \end{cases} \quad (13)$$

where k is the period-dependent coefficient; and $Z_{2.5}$ (km) is the depth to the 2.5 km/sec shear-wave velocity horizon beneath the site (sediment depth).

5.6. Hanging wall term (f_{hng})

Before the 1980's, the Hanging Wall (HW) effect was known as a geometrical effect caused by the asymmetry of dipping fault. By increasing the number of recorded ground motions at short distance of causative faults, empirical residuals and the rock simulations demonstrated a stronger HW effect than expected. This effect has been known as one of the important characteristics of near-fault ground motions after 1994 Northridge and the 1999 Chi-Chi earthquakes, Abrahamson and Somerville [20].

The recoded data at near-fault zone ($R_{\text{rup}} \le 25$ km) showed that the PGAs on the hanging wall were much greater than those on the footwall at the same R_{rup} [5]. Further analysis and observation indicated larger values of Peak Ground Velocity (PGV) and Peak Ground Displacement (PGD) on the hanging wall [21].

Herein, the function introduced by Chiou and Youngs [22] is used to model hanging-wall effects. In this function, the hanging-wall effects have a smooth transition from the hanging wall to the footwall blocks:

$$f_{\text{hng}} = a_{13}(T) f_{\text{hng},R} f_{\text{hng},M} f_{\text{hng},Z} f_{hng,\delta}. \quad (14)$$

Each term in Eq. (14) are piecewise linear complicated functions for distance ($f_{\text{hng},R}$), magnitude ($f_{\text{hng},M}$), depth-to-top rupture ($f_{\text{hng},Z}$), and dip ($f_{\text{hng},\delta}$).

HW effect decreases with an increase in distance; thus, Chiou and Youngs [22] used R_{jb} and R_{rup} to simulate the reduction. The Joyner and Boore distance is a measure from site to the HW:

$$f_{hng,R} = \begin{cases} 1 & R_{jb} = 0 \\ \frac{\left[\max\left(R_{\text{rup}}, \sqrt{R_{jb}^2+1}\right) - R_{jb}\right]}{\max\left(R_{\text{rup}}, \sqrt{R_{jb}^2+1}\right)} & R_{jb} > 0, Z_{\text{top}} < 1 \\ \frac{R_{\text{rup}} - R_{jb}}{R_{\text{rup}}} & R_{jb} > 0, Z_{\text{top}} \ge 1 \end{cases} \quad (14.1)$$

where R_{jb} (km) is the distance nearest to the surface projection of the co-seismic rupture plane (Joyner-Boore distance).

Based on the survey on residuals, there is a stronger dependency between HW and magnitude than between HW and dip:

$$f_{\text{hng},M} = \begin{cases} 0 & M_w \le 6.0 \\ 2(M_w - 6.0) & 6.0 < M_w < 6.5 \\ 1 & M_w \ge 6.5 \end{cases} \quad (14.2)$$

Z_{top} is a factor that Campbell and Bozorgnia added to the function to have a soft transition from the hanging wall to the footwall, even for small Z_{top}:

$$f_{\text{hng},Z} = \begin{cases} 0 & Z_{\text{top}} \ge 20 \\ \frac{20 - Z_{\text{top}}}{20} & 0 \le Z_{\text{top}} < 20 \end{cases} \quad (14.3)$$

where Z_{top} (km) is the depth from the top of the co-seismic rupture plane.

According to residuals, there is no strong dependency between HW and dip; however, for the dip angle not equal to 90 degrees, HW amplification should not be included. The following equation tries to reduce and finally extinct HW effect for dip angles greater than 70 degrees:

$$f_{\text{hng},\delta} = \begin{cases} 1 & \delta \leq 70 \\ \frac{90-\delta}{20} & \delta > 70 \end{cases} \quad (14.4)$$

where $\delta(^\circ)$ is the angle of the fault plane (dip).

5.7. Depth-to-top rupture model ($f_{Z\,top}$)

Empirical and theoretical evidences show that when the ground surface above seismic source is broken during earthquake, the recorded ground motions generally have lower amplitude than the earthquakes with hidden faults [23]. Dynamic rupture simulations show that if a weak zone exists at shallow depths, rupture of the shallow part of the fault will be controlled by velocity strengthening. The other consequences of existing weak zone are larger slip weakening distances, larger fracture energy, larger energy absorption from the crack tip, lower rupture velocity, and lower slip velocity at greater depths on the fault. These lead to lower ground motions for surface faults rather than for buried or hidden faults.

Recent studies indicate that there is a correlation between magnitude and depth-to-top rupture [23]. They show that large earthquakes tend to rupture to the surface whereas in small earthquakes, they tend to be at depth [24].

To address this correlation, Abrahamson and Silva [24] showed that the inter-event residuals were a function of depth-to-top rupture.

So as to limit the effect of this positive correlation on the relation studied in the current paper, only records from $5 \leq M_w \leq 6$ are used to derive depth-to-top rupture (Z_{top}) dependency.

Abrahamson and Silva [24] used a piecewise linear function to show the depth-to-top dependency on different magnitudes. This function is employed in this part to determine the depth-to-top rupture:

$$f_{Z_{\text{top}}} = \begin{cases} \left(\frac{a_{14}(T)*Z_{\text{top}}}{10}\right) & Z_{\text{top}} \leq 10 \text{ km} \\ a_{14}(T) & 10 \text{ km} \leq Z_{\text{top}} \end{cases} \quad (15)$$

where Z_{top} (km) is the depth from the top of the co-seismic rupture plane.

5.8. Rupture dip term (f_{dip})

Recent research indicates the influence of Dip (angle of the fault plane) on ground motion [1]. As per the results of the present study, the recorded ground motion has a larger amplitude in earthquakes with higher dip angles; this effect decreases by increase in magnitude. This effect has previously been indicated by Campbell and Bozorgnia [1], who used linear multi-criteria function in the recent attenuation relation. This function is defined as:

$$f_{\text{dip}} = \begin{cases} a_{15}(T)\delta & M_w < 4.5 \\ a_{15}(T)(5.5 - M_w)\delta & 4.5 \leq M_w \leq 5.5 \\ 0 & M_w > 5.5 \end{cases} \quad (16)$$

6. Regression results

The present study determines the median ground motion model coefficients for peak ground acceleration and spectral acceleration for 5% critical damping ratio and 21 oscillator periods ranging in 0.01-10.0 s, which are listed in Table 4. The aleatory standard deviations and combined uncertainty coefficients are listed in Table 5. It is worth to note that the constants $c_1 = 6.5$ and $n = 2$ are the same for all oscillator periods.

Different distributions of records with respect to the independent variables cause period-to-period variability. This variability may be reduced by smoothing the derived coefficients. This method improves reliability of the equation, especially in long-period estimates due to the existence of fewer records than those in the short-period region [8].

Because of the relatively uniform distribution of recordings with respect to magnitude and distance, none of them were weighed during regression analysis (Figure 1). However, in very long periods (7.5-10 sec), un-weighed regression showed a large variation between the derived coefficients in two periods. This indicates that using a simple function for smoothing the coefficient is not sufficient for wide-range periods.

7. Results of the empirical model

Results of the empirical model for bed rock ($V_{s30} =$ 760 m/s) and soil deposit ($V_{s30} = 270$ m/s) are plotted in Figures 2 and 3, respectively. These figures show the decay of estimated peak ground acceleration and spectral acceleration at 0.1, 1, and 3 sec of natural periods. In these figures, the variation of acceleration versus distance has been displayed for two different magnitudes ($M_w = 5.5$ and 7.0) and four faulting styles (strike-slip, normal, oblique, and reverse). As shown, the effects of earthquake magnitude and fault style on spectral acceleration are reduced by increasing the period; nevertheless, this decrement is of lower degree for large-magnitude events.

Figure 4 shows the significant difference of spectral accelerations with different fault mechanisms in short and median periods. This difference decreases by

Table 4. Coefficients and statistical parameters from the regression analysis of PGA and PSA (T_1).

T (sec)	a_1	a_2	a_3	a_4	a_5	a_6	a_7	a_8	a_9	a_{10}	a_{11}	a_{12}	a_{13}	a_{14}	a_{15}	k
PGA	1.846	-0.244	-0.06	-0.144	-1.103	0.058	8.623	-0.303	-0.120	0.129	0.000	0.343	0.332	0.540	-1.586	1.839
0.01	1.850	-0.032	-0.060	-0.144	-1.101	0.058	8.607	-0.305	-0.124	0.128	0.000	0.340	0.332	0.550	-1.658	1.839
0.02	1.730	-0.041	-0.047	-0.132	-1.085	0.072	7.980	-0.313	-0.126	0.124	0.000	0.350	0.388	0.562	-1.934	1.840
0.03	1.644	-0.077	-0.021	-0.103	-1.087	0.102	7.584	-0.322	-0.160	0.148	-0.001	0.421	0.420	0.532	-0.780	1.841
0.05	1.469	-0.156	0.019	-0.083	-1.000	0.110	6.761	-0.360	-0.233	0.165	-0.001	0.656	0.450	0.332	0.331	1.843
0.075	1.513	-0.230	0.061	-0.053	-0.978	0.125	7.057	-0.395	-0.252	0.200	-0.001	0.844	0.430	0.225	2.833	1.845
0.1	1.745	-0.262	0.077	-0.077	-0.956	0.081	8.244	-0.405	-0.223	0.196	-0.001	0.952	0.402	0.124	2.206	1.847
0.15	2.236	-0.249	0.071	-0.086	-1.023	0.078	9.722	-0.374	-0.224	0.159	-0.001	0.902	0.416	0.230	-1.711	1.852
0.2	2.498	-0.231	0.070	-0.124	-1.032	0.053	9.763	-0.300	-0.226	0.148	-0.001	0.850	0.389	0.228	0.161	1.856
0.25	2.241	-0.209	0.073	-0.121	-0.992	0.063	8.884	-0.288	-0.177	0.178	-0.001	0.742	0.428	0.216	0.704	1.861
0.3	2.225	-0.182	0.057	-0.130	-1.006	0.070	8.544	-0.281	-0.133	0.189	-0.001	0.645	0.414	0.289	2.141	1.865
0.4	1.971	-0.163	0.043	-0.133	-1.005	0.074	7.437	-0.171	-0.021	0.281	-0.001	0.609	0.462	0.184	1.296	1.874
0.5	1.967	-0.136	0.033	-0.144	-1.067	0.078	7.885	-0.023	0.038	0.283	-0.001	0.564	0.469	0.222	1.346	1.883
0.75	1.504	-0.112	0.017	-0.118	-1.079	0.106	7.615	-0.055	0.093	0.289	0.000	0.498	0.573	0.061	0.564	1.906
1.0	1.437	-0.087	-0.003	-0.144	-1.107	0.082	7.957	0.013	0.169	0.348	0.000	0.423	0.558	-0.157	1.139	1.929
1.5	1.554	-0.067	-0.014	-0.229	-1.171	0.020	9.083	-0.107	0.203	0.384	0.000	0.358	0.474	-0.379	3.749	1.974
2.0	1.556	-0.094	0.004	-0.253	-1.249	0.019	11.140	-0.083	0.213	0.419	0.000	0.416	0.518	-0.670	4.401	2.019
3.0	1.451	-0.130	0.030	-0.318	-1.292	-0.011	12.814	-0.254	0.269	0.417	0.000	0.441	0.362	-1.109	5.056	2.110
4.0	0.962	-0.156	0.050	-0.343	-1.255	0.019	12.808	-0.289	0.265	0.347	0.000	0.478	0.164	-1.237	6.265	2.200
5.0	1.211	-0.150	0.067	-0.406	-1.346	0.008	14.658	-0.458	0.214	0.196	0.000	0.457	0.144	-1.243	6.819	2.291
7.5	1.013	-0.188	0.092	-0.441	-1.438	0.061	17.159	-0.695	0.118	-0.092	-0.001	0.397	0.132	-1.051	8.697	2.517
10	-0.228	-0.163	0.082	-0.414	-1.330	0.100	15.025	-0.626	0.136	-0.098	-0.001	0.315	0.166	-0.926	9.116	2.744

Table 5. Aletory uncertainties. (σ: intra-event uncertainty; τ: inter-event uncertainty; $\sqrt{\sigma^2+\tau^2}$): combined uncertainty).

T (sec)	Standard deviation		Geometric mean
	σ_{logy}	τ_{logy}	σ_{total}
PGA	0.496	0.240	0.551
0.01	0.493	0.221	0.540
0.02	0.502	0.236	0.555
0.03	0.533	0.260	0.593
0.05	0.526	0.312	0.612
0.075	0.536	0.338	0.634
0.1	0.521	0.353	0.629
0.15	0.511	0.316	0.601
0.2	0.498	0.291	0.577
0.25	0.492	0.270	0.561
0.3	0.508	0.246	0.565
0.4	0.530	0.220	0.574
0.5	0.537	0.189	0.569
0.75	0.571	0.195	0.603
1.0	0.586	0.194	0.617
1.5	0.597	0.189	0.626
2.0	0.604	0.199	0.636
3.0	0.608	0.206	0.641
4.0	0.593	0.228	0.635
5.0	0.595	0.227	0.637
7.5	0.583	0.319	0.665
10	0.578	0.276	0.641

increasing the period for both rock and soil sites. The average ratio of the spectral accelerations of reverse fault to strike-slip varies between 0.9 $\sim$ 1.45. This ratio is in compliance with previously reported ratios by different authors who recommended a maximum factor of 1.3.

In short-period ranges, spectral accelerations on rock site are higher than those on soil site; however, they maintain a reverse order in long periods.

Figure 5 depicts that in short-period ranges, the spectral acceleration recorded on soft clay ($V_{s30} = 180$) has the lowest value in comparison with those on other sites. This is mainly due to the nonlinear behavior of soft soil in short-period ranges and lack of data recorded on this site. By increasing the period, the attenuation relation of soft clay will have a similar trend to that of the stiff soil ($V_{s30} = 270$). Firm rock ($V_{s30} = 1130$) and hard rock ($V_{s30} = 1500$) diagrams show a reduction by increasing the period as there is no soil in these sites. As shown by this figure, due to reverse-fault earthquakes, the spectral acceleration has higher amplitude than the strike-slip and normal faulting ground motions.

As explained before, the effect of different sediment depths is represented by $Z_{2.5}$. Figure 6 delineates the effect of this parameter on spectral acceleration. Amplification of spectra has proportional relation to sediment depth growth. As shown, because of nonlinear effect of soil, the site response is less dependent on elastic properties and curves are very close to each

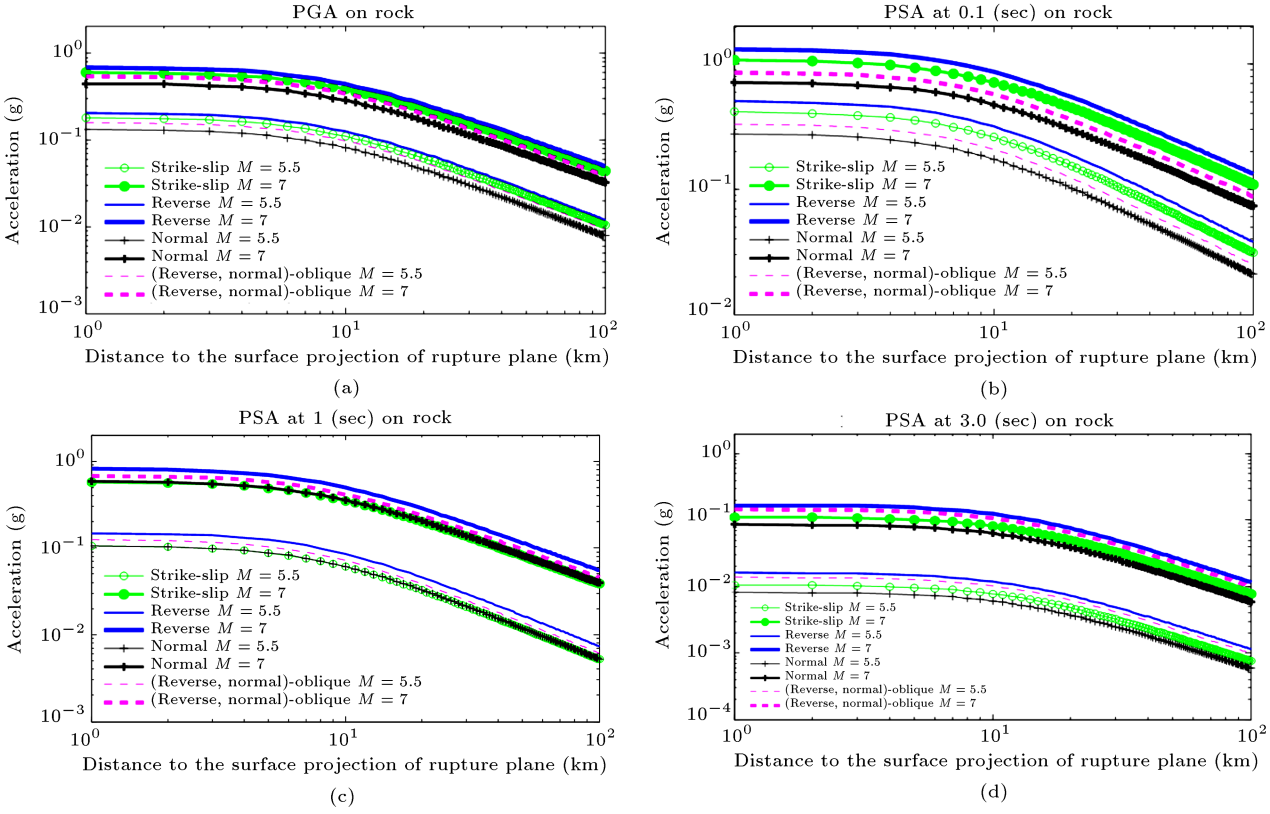

Figure 2. Ground-motion relations in this study for strike-slip, reverse, and normal faulting for rock site ($V_{s30} = 760$ m/s): (a) Corrected PGA, (b) PSA (T_1) at 0.1 sec, (c) PSA (T_1) at 1.0 sec, and (d) PSA (T_1) at 3.0 sec.

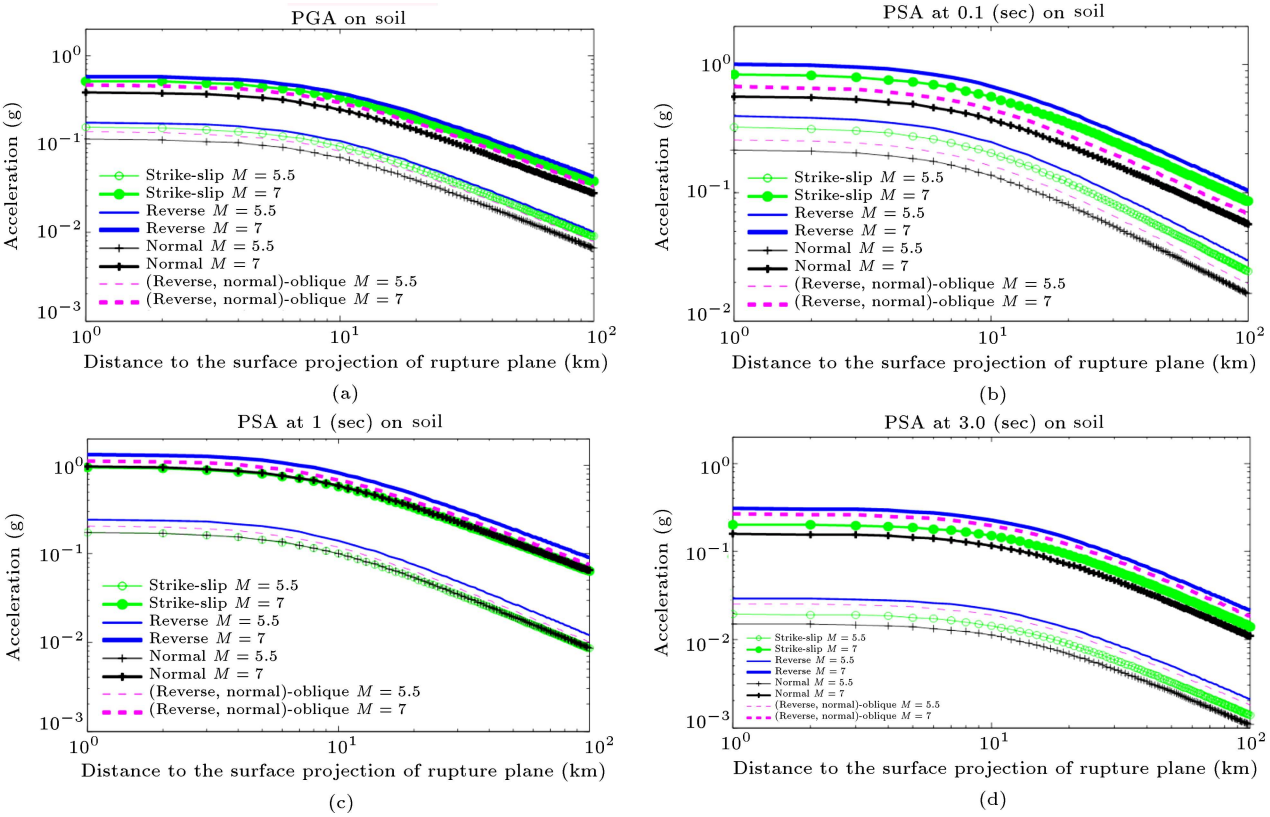

Figure 3. Ground-motion relations in this study for strike-slip, reverse, and normal faulting for soil site ($V_{s30} = 270$ m/s): (a) Corrected PGA, (b) PSA (T_1) at 0.1 sec, (c) PSA (T_1) at 1.0 sec, and (d) PSA (T_1) at 3.0 sec.

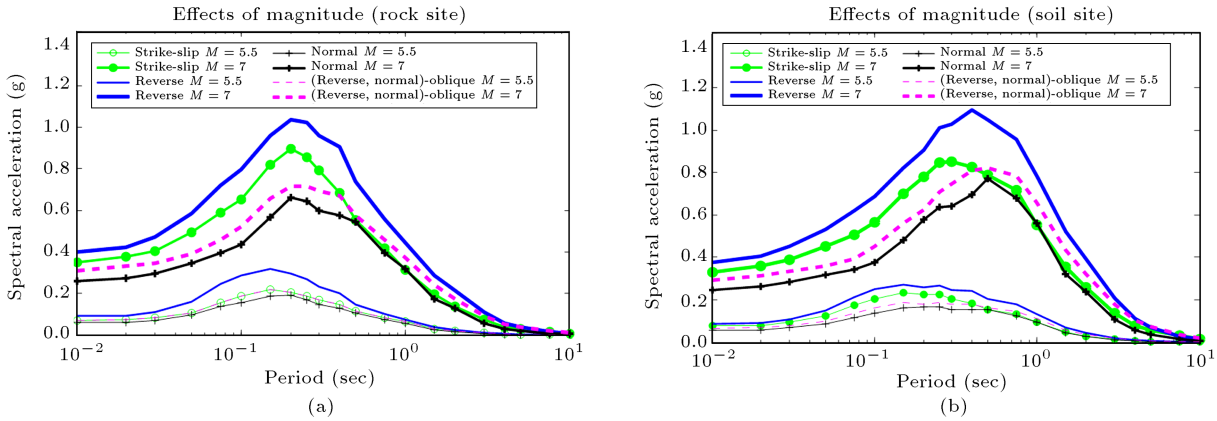

Figure 4. PSA (T_1) (5% damping) predicted by the ground-motion relations developed in this study, showing the effects of (a) magnitude on the rock site, $V_{s30} = 760$ m/s, and (b) magnitude on the soil site, $V_{s30} = 270$ m/s. It is worth to note that the spectra are evaluated for $M_w = 7.0$ and $M_w = 5.5$ in distance $R_{\text{rup}} = 10$ km for strike-slip, reverse, and normal faulting.

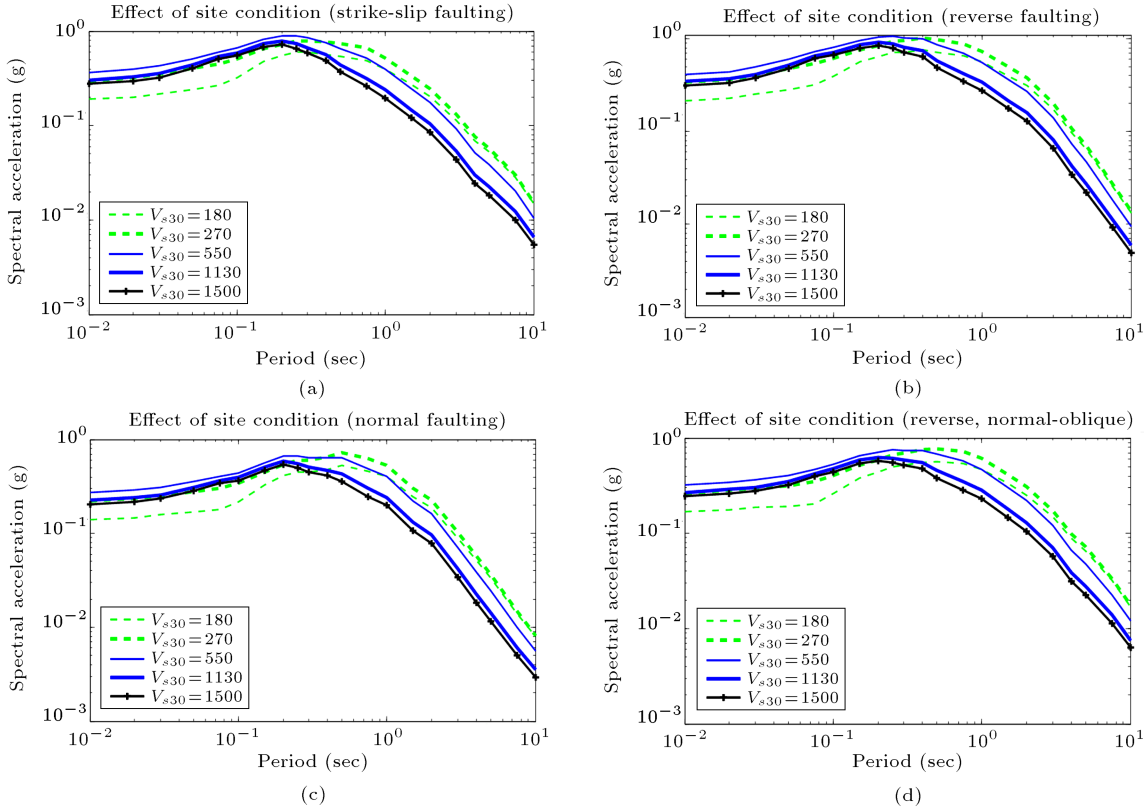

Figure 5. PSA (T_1) (5% damping) predicted by the ground-motion relations developed in this study, showing the effects of faulting mechanism: (a) Reverse, (b) strike-slip, (c) normal, and (d) oblique for different local soil conditions for the horizontal component of ground motion; the spectra are evaluated for $M_w = 7.0$ and $R_{\text{rup}} = 10$ km.

other in short-period ranges. However, the amplitude of PSA (T_1) increases in proportion to base sediment depth for long periods.

8. Comparison with previous studies

8.1. Comparison with NGA equations

This part compares the ground motion relation proposed in this study with four NGA ground motion relations that are widely used to estimate horizontal response spectra for seismological and engineering analyses. These four equations have been introduced by Campbell and Bozorgnia [1], Ambraseys and Douglas [9], Boore and Atkinson [17], and Abrahamson and Silva [24].

All the relations are derived using the average

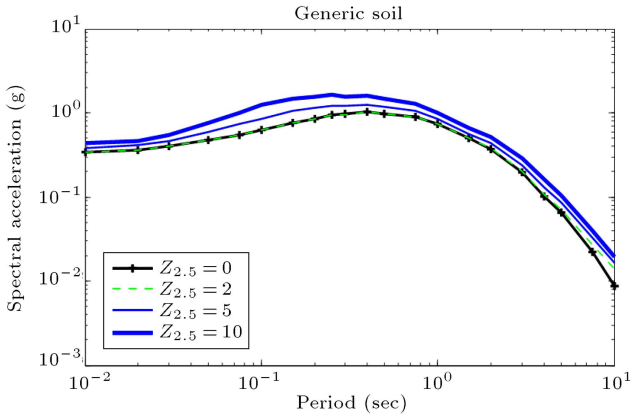

Figure 6. Summary of results from the basin response simulations based on different sediment depths. On depth to the $V_s = 2.5$ km/s isosurface from our study.

horizontal components for both soil and rock. They all use different definitions for local site conditions. Rock in Abrahamson and Silva [24] equation is defined as a deposit with less than 20 m of soil overlying rock. Boore and Atkinson [17] used the velocity parameter, V_{s30} for classifying generic soil and rock in accordance with NEHRP Provision.

Ambraseys and Douglas [9] employed a linear function to indicate the site effect. This type of classification leads to inaccurate results, especially for soft-clay-soil sites or saturated sandy sites, because nonlinearity is not considered in the site response, Choi and Stewart [18]. In other attenuation relations, the site condition is modeled by using a function with two linear and nonlinear components.

Campbell and Bozorgnia [1] use seismogenic distances (R_{jb}, and $R_{\rm rup}$) rather than distance to the surface projection of the fault (R_{jb}), which has been employed by Ambraseys and Douglas [9] and Boore and Atkinson [17]. As described before, the shortest distances to the rupture plane ($R_{\rm rup}$) were selected by Abrahamson and Silva [24] as well as this study. To compare all these equations, it is necessary to use a unified distance.

Figure 7 compares the predicted median spectral acceleration of four NGA equations with ground motion relations proposed in this study. This comparison has been performed for a site located at 10 km from a reverse fault and for earthquakes of $7M_w$ on rock and soil site. The effect of hanging wall has been ignored in this figure as it was not considered in some equations.

As shown, the proposed attenuation relation is relatively higher than those in other NGA equations at median and long-period ranges. This can be explained by the selected domains for the distance ($R_{\rm rup} \leq 60$) and magnitude ($5.2 \leq M_w \leq 7.9$), which are in compliance with near-field data set in this study. In fact, the long-period acceleration dominates and amplifies the response of spectra in this range of magnitude.

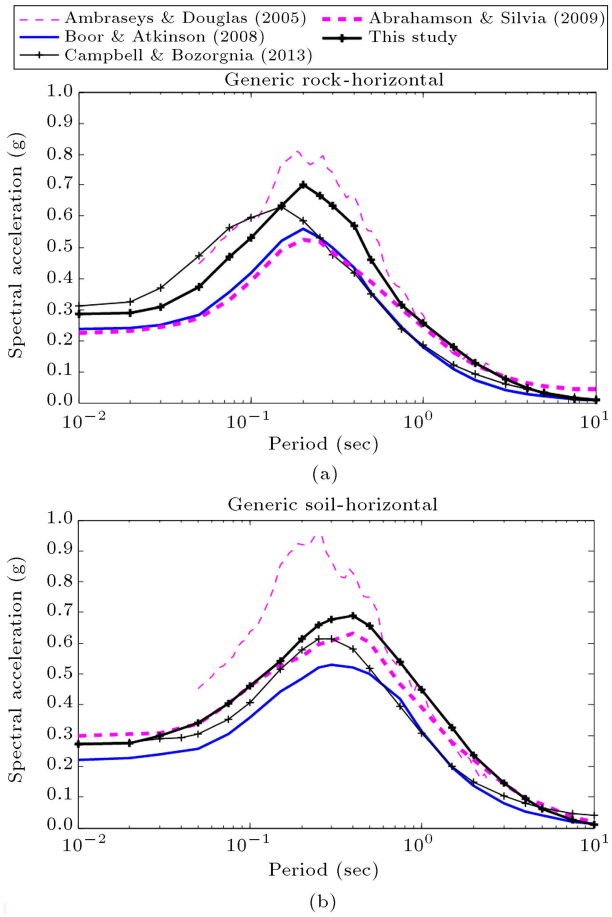

Figure 7. Comparison of the predicted PSA(T_1)s (5% damping) (a) for generic rock with $V_{s30} = 760$ m/s and (b) for generic soil with $V_{s30} = 270$ m/s by the ground-motion relation in this study and five ground-motion relations widely used in seismology and engineering. The spectra are evaluated for no HW, $M_w = 7.0$, $R_{JB} = R_{\rm rup} = 10$ km.

Among the described NGA equations, the hanging wall effect has been considered by only two authors. Figure 8 shows that the effect of hanging wall for rock site is higher than that for soil sites in [1,24]; however, hanging wall does not have a specific relation with site condition in near-field in the equation proposed in this study. The comparison of Figure 8 with Figure 7 indicates that the effect of hanging wall magnifies the spectral acceleration in short and medium periods; however, its influence decreases at long-period ranges.

Figure 9 compares the horizontal standard deviations of different attenuation relations for $M_w = 7$ and $R = 10$ km. Standard deviations contribute significantly to deterministic and probabilistic estimates of ground motion. Among different attenuation relations, the standard deviation of Ambraseys and Douglas equation [4] is the only magnitude-dependent relation. As illustrated, the standard deviation of attenuation relation proposed in this study decreases significantly

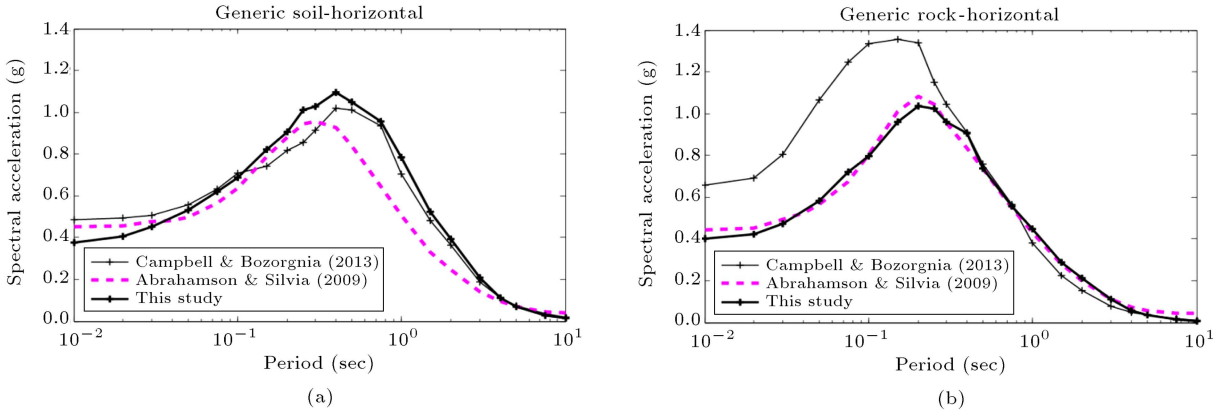

Figure 8. Comparison of the predicted PSA(T_1)s (5% damping) (a) for generic rock with $V_{s30} = 760$ m/s and (b) for generic soil with $V_{s30} = 270$ m/s by the ground-motion relation in this study and five ground-motion relations widely used in seismology and engineering. The spectra are evaluated for HW, $M_w = 7.0$, $R_{JB}, R_{\rm rup} = 10$ km.

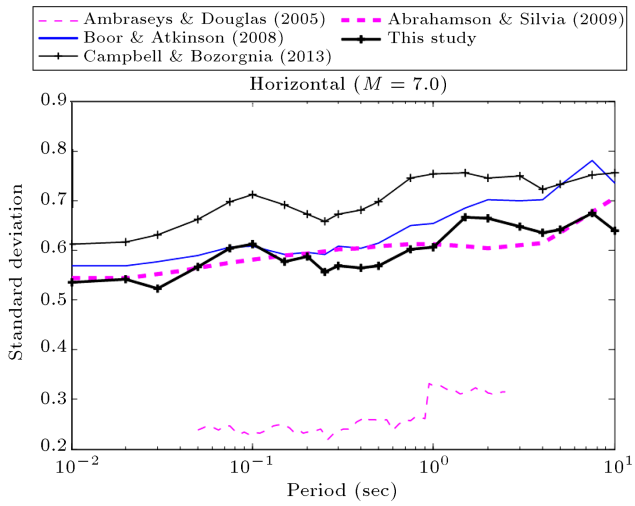

Figure 9. Comparison of the predicted standard deviations of spectral acceleration ($\sigma_{\rm logy}$) by this study and five ground-motion relations widely used in seismology and engineering. The standard deviations are evaluated for $M_w = 7.0$.

by removing unreliable data and employing stable algorithm for regression.

The intra-event residuals were normalized by $\sigma_{\rm total}$ in order to better imagine the relative differences in the scatter in the intra-event residuals among the different strong-motion parameters. For the model to be unbiased, the intra-event residuals should have zero mean and be un-correlated with respect to the parameters in the regression model. Figure 10 indicates that the regression models are unbiased with respect to distance parameter.

8.2. Comparison with Iran plateau attenuation relations

Previously developed attenuation relations for Iran plateau consisted of only few simple functions by using plain regression methods. Many attenuation relations have recently been introduced based on recorded data in this region. These equations were developed by adding new terms, such as style-of-faulting and site effect, and advanced regression methods and nonlinear functions were used in the process of their mathematical model to simulate their parameters. The distinct factors of these relations can be summarized as follows:

- Application of different distance types and intervals;
- Different types of magnitude parameters;
- Different methods employed for data filtering;
- Different methods employed for regression.

The main problem that is common among all equations is the presence of unreliable records in their data sets. Further, because of the small and moderate size of events that have been used in these equations, the causative faults are not known for many earthquakes. Accordingly, the erratic hypo-central distance ($r_{\rm hpyo}$) is chosen by most of these equations.

These equations generally face lack of reliable records in their data sets. For example, unknown causative faults for many earthquakes drive most of authors to use the erratic hypo-central distance ($r_{\rm hpyo}$) in most of these equations. Furthermore, many authors use the S-P method to derive $r_{\rm hpyo}$ because of uncertainty in reported hypo-central locations.

One of the major differences between recently developed attenuation relations for NGA and Iran is in the number of observed large-magnitude ground motions at small-to-moderate distance of seismic source. For this reason, the recently developed equations for Iran cannot appropriately predict near-field ground motions.

In this part, the attenuation relations that were extended for Iran plateau since 1994 are compared with relations introduced in this study. These equations

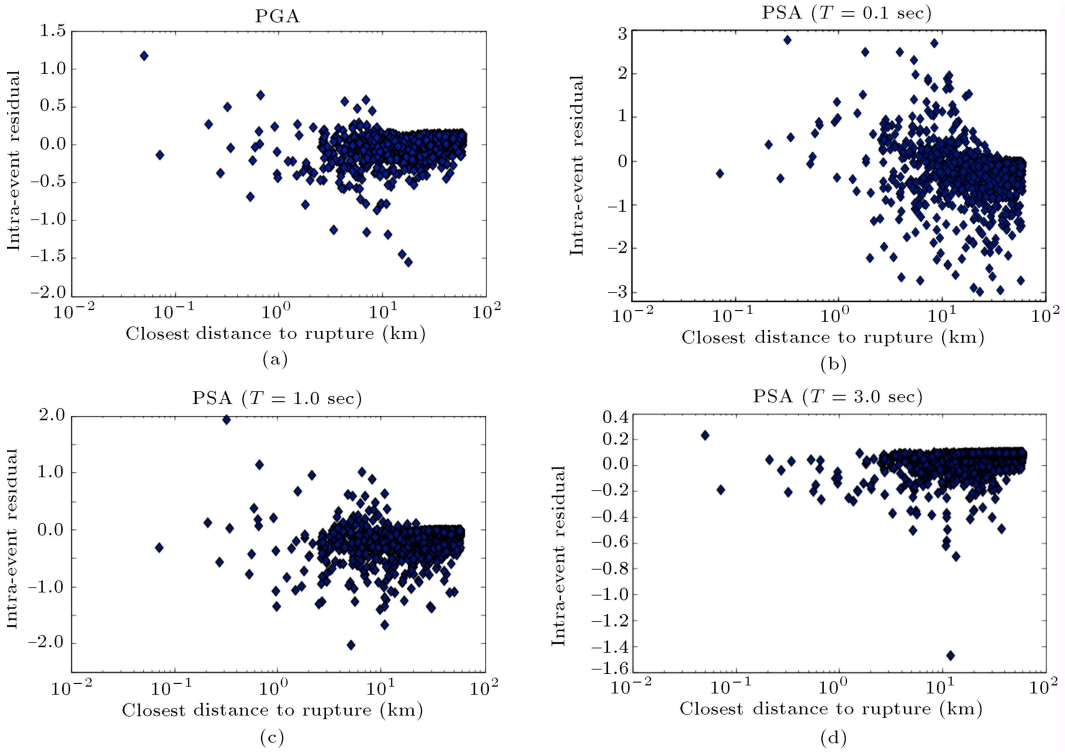

Figure 10. Ground motion extra-event residuals as a function of distance for the regression analysis of the average horizontal component of ground motion: (a) PGA, (b) PSA at 0.1 sec, (c) PSA at 1.0 sec, and (d) PSA at 3.0 sec.

have been introduced by Ramazi and Schenk [25], Zaré et al. [26], Khademi [27], Nowroozi [28], Mahdavian [29], Zaré and Sabzali [30], Aghabarati and Tehranizadeh [31], and Ghodrati et al. [32,33]. This comparison shows the level of consistency of these equations with near-filed specific equation, which has been derived from recent data collected across the world.

In these relations, focal distance has been selected as distance parameter and average focal depth is assumed to be 20 km. Khademi's equation [27] is the only exception, which has used R_{rup} and, as shown later, this causes great errors in short distances.

Rock in Ramazi and Schenk's equation [25], is defined as a deposit with less than 10 m of soil overlying bed rock. There is no general consensus among scientists on this definition. Zaré et al. [26] used four site categories, which were based on H/V receiver function measurements. Their dataset contained only two near-field records (less than 10 km) from earthquakes with magnitudes of $M_w > 6.0$ and focal depths varying between 9 and 133 km.

In Khademi's equation [27], the standard deviation is PGA-dependent and individual record deviation has been computed but not according to the standard procedure.

At preliminary assumptions of Nowroozi's equation [28], three terms, namely, $c_5(M_w - 6)^2$, c_6 EPD, and c_7F, were included; however, they were omitted from the final equation presented. c_7 F term referred to faulting mechanism, which was omitted from equation due to lack of information. Two other items were also omitted as soon as they were found statistically insignificant. The selected magnitude events for this equation were mainly less than 5.

Mahdavian [29] divides Iran into two regions, Zagros region and the rest of Iran; however, due to lack of data (only 15 records) for estimation of Zagros and soil sites, large standard deviation has been incorporated into this equation. Some records in the data set do not feature the main portion of shaking.

In Zare and Sabzali equation [30], lack of near-field records limits its application to far fields. As shown in Figure 11, the predicted motions for rock (V_{s30} = 760 m/s) and soil (V_{s30} = 270 m/s) by this equation are similar, which make it unreliable in some features.

Aghabarati and Tehranizadeh [31] used three mechanism classes and V_{s30} to characterize site conditions. Due to monotonic variation of constraint c_7 (T) with period, its spectral acceleration has sudden changes at short-period ranges. To show depth-to-top effect, they used two terms for reverse and strike-slip earthquakes. To define the functional form for hanging wall effect, they used residuals from one-dimensional simulation. Examination of normalized inter- and intra-event residuals against M_w, distance, mechanism, and other parameters shows no bias in trends.

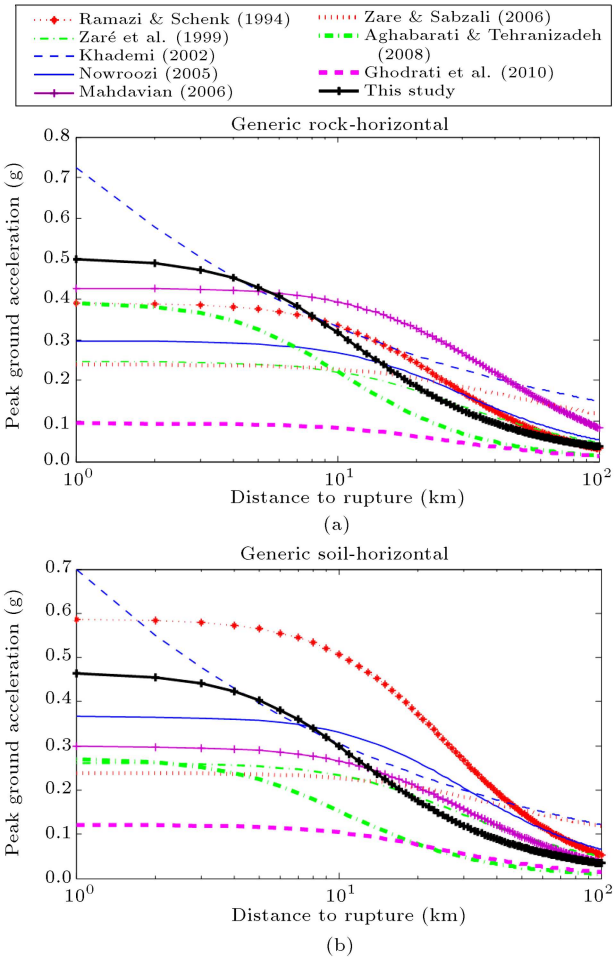

Figure 11. Comparison between the predicted PGAs for generic soil on the hanging wall by this study and nine horizontal ground-motion relations that were extended for Iran. Generic rock is defined in the text, but generally represents sites with (a) $V_{s30} = 760$ m/s and (b) $V_{s30} = 270$ m/s. The relations are evaluated for $M_w = 7.0$, $h = 20$, and a reverse or thrust fault dipping at 45 degrees.

Ghodrati A. et al. [33] used V_{s30} for classification of site to rock and soil (soil, $V_{s30} < 375$ m/s and rock $V_{s30} > 375$ m/s). The considered focal depth in this equation equaled 5 km while this parameter was of an average of 22 km in their dataset. This relation was developed based on reappraised dataset, which had been already introduced in Ghodrati Amiri et al. (2007b) [32] equation.

Figure 11 compares the predicted PGAs of the above-mentioned equations for earthquake events with magnitudes of $M_w = 7.0$ and $M_s = 7.04$ from reverse fault without considering hanging-wall effect. As illustrated by the figure, Aghabarati and Tehranizadeh attenuation relation [31] has a trend similar to that in the equation proposed in the present study, which is due to similarities in some functions and parameters used in both relations. Figure 11 shows that application of simple coefficient for modeling the site effect is not an appropriate procedure. For instance, this coefficient for two sites is the same in Zare and Sabzali equation [30]. Since Mahdavian [29] and Ghodrati et al. [33] used M_s as magnitude parameter, their relation is not applicable to magnitudes greater than 7.8.

As expected, the greatest difference between the equation presented in this study and other equations is observed in short-distance ranges. In this range and on rock site, Mahdavian [29] equation, and on soil site Nowroozi's equation [28] are similar to the equation proposed by this study. In close distances, Khademi's equation [27] exhibits a trend different from the ones shown by other equations.

9. Conclusion

The ground motion relations developed in this study prove to be valid for estimation of Peak Ground Acceleration (PGA) and 5% damped Pseudo Spectral Acceleration (PSA(T_1)) for shallow crustal earthquakes with magnitudes between 5.2 and 7.9 and distances smaller than 60 km.

We considered our ground motion relations to supersede previous relations, but a new algorithm and new combination of parameter functions were used in regression analyses, which were selected based on fairly good performance of data. Genetic algorithm was also used to obtain optimum variances of the residuals. With these proceedings, we could reduce the error to an acceptable value. A new set of data that included the data of previous works plus data that had been approved by the recent research was employed for extending the attenuation relation.

The study explicitly addresses such topics as sediment depth and the use of NEHRP site classes. Moreover, hanging wall effects, dividing faulting mechanism to four main categories (reverse, strike-slip, oblique, and normal faulting), sediment depth effect, depth-to-top rupture effects, and finally nonlinear soil response were considered in the introduced equation. Some of the important achievements of this study can be summarized as:

1. The equation is affected by near-field effect and in long-period range, the spectral accelerations are higher than those in similar studies;
2. Hanging wall effect magnifies spectral acceleration in near-field on rock and soil sites, but the magnification factor on soil sites is clearly higher;
3. In short-period ranges, the spectral acceleration recorded on soft clay ($V_{s30} = 180$) has the lowest value in comparison with other sites. This is due to the nonlinear behavior of soft soil in short-period ranges and lack of data recorded on this site. By increasing period, the attenuation relation of soft

clay will exhibit a similar trend to that of stiff soil ($V_{s30} = 270$). Firm rock ($V_{s30} = 1130$) and hard rock ($V_{s30} = 1500$) diagrams show a downward trend due to lack of soil on these sites;

4. Sediment depth has a significant impact on the amplitude of ground motion, specifically in medium and long periods;
5. Spectral accelerations in short-period ranges are controlled by earthquake magnitude and style-of-faulting; however, in long periods, less dependency can be observed;
6. In comparison with other NGA relations, the standard deviation of the attenuation relation proposed in this study decreases significantly by removing unreliable data and employing stable algorithm for regression;
7. The residual analysis of the derived attenuation relations for Iran plateau shows that small changes in distance parameter will have a significant impact on the predicted acceleration;
8. The data sets and functions selected for most of the attenuation relations of Iran plateau are almost identical; but, there is a great difference between their attenuation curves. This can be due to using unreliable data, linear function, and simple methods for regression.

References

1. Campbell, K.W. and Bozorgnia, Y., *NGA-West2 Ground Motion Model for the Horizontal Components of PGA, PGV, and 5%-Damped Elastic Pseudo-Acceleration Response Spectra for Periods Ranging from 0.01 to 10 sec*, PEER (2013).
2. Boore, D.M., Stewart, J.P. and Atkinson, G.M., *NGA-West2 Equations for Predicting Response Spectral Accelerations for Shallow Crustal Earthquakes*, PEER (2013).
3. Campbell, K.W. and Bozorgnia, Y. "Updated near-source ground-motion (attenuation) relations for the horizontal and vertical components of peak ground acceleration and acceleration response spectra", *Bulletin of Seismological Society of America*, **93**(1), pp. 31-314 (2003).
4. Ambraseys, N.N. and Douglas, J. "Near-field horizontal and vertical earthquake ground motions", *Soil Dynamic and Earthquake Engineering*, **23**(1), pp. 1-18 (2003).
5. Abrahamson, N.A. and Silva, W.J. "Empirical response spectral attenuation relations for shallow crustal earthquakes", *Seismological Research Letters*, **68**(1), pp. 94-127 (1997).
6. Campbell, K.W. and Bozorgnia, Y., *NGA Ground Motion Relations for the Geometric Mean Horizontal Component of Peak and Spectral Ground Motion Parameters*, PEER, pp. 4-112 (2008).
7. Ancheta, T.D., Darragh, R.B., Stewart, J.P., Silva, W.J., Chiou, B.S.J., Wooddell, K.E., Graves, R.W., Kottke, A.R., Boore, D.M., Kishida, T. and Donahue, J.L., *PEER NGA-West2 Database*, PEER (2013).
8. Shokran, A.N. and Taghikhany, T. "Prediction equations for generalized interstory drift spectrum considering near-fault ground motions", *Natural Hazards*, **80**(3), pp. 1443-1473 (2016).
9. Ambraseys, N.N. and Douglas, J. "Equations for the estimation of strong ground motions from shallow crustal earthquakes using data from Europe and the middle east, horizontal peak ground acceleration and spectral acceleration", *Bulletin of Earthquake Engineering*, **3**(1), pp. 1-53 (2005).
10. Spudich, P., Joyner, W.B., Lindh, A.G., Boore, D.M., Margaris, B.M. and Fletcher, J.B. "A revised ground motion prediction relation for use in extensional tectonic regimes", *Bulletin of Seismological Society of America*, **89**(5), pp. 1156-1170 (1999).
11. Boore, D.M., Joyner, W.B. and Fumal, T.E. "Equations for estimating horizontal response spectra and peak acceleration from western North American earthquakes: a summary of recent work", *Seismological Research Letters*, **68**(1), pp. 53-128 (1997).
12. Abrahamson, N.A. and Youngs, R.R. "A stable algorithm for regression analyses using the random effects model", *Bulletin of the Seismological Society of America*, **82**(1), pp. 505-510 (1992).
13. Brillinger, D.R. and Preisler, H.K. "Further analysis of the Joyner-Boore attenuation data", *Bulletin of Seismological Society of America*, **75**(2), pp. 611-614 (1985).
14. Sadigh, K., Chang, C.Y., Egan, J.A., Makdisi, F. and Youngs, R.R. "Attenuation relationships for shallow crustal earthquakes based on California strong motion data", *Seismological Research Letters*, **68**(1), pp. 180-189 (1997).
15. Youngs, R.R. "Soil amplification and vertical to horizontal ratios for analysis of strong motion data from active tectonic region", *Appendix 2C in Guidelines for Determining Design Basis Ground Motions: Appendices for Ground Motion Estimation,* **68**(1), pp. 102-293 (1993).
16. Bazzurro, P. and Cornell, C.A. "Nonlinear soil-site effects in probabilistic seismic-hazard analysis", *Bulletin of the Seismological Society of America*, **94**(6), pp. 2110-2123 (2004).
17. Boore, D.M. and Atkinson, G.M. "Ground-motion prediction equations for the average horizontal component of PGA, PGV, and 5%-damped PSA at spectral periods between 0.01 s and 10.0 s", *Earthquake Spectra*, **24**(1) pp. 99-138 (2008).
18. Choi, Y. and Stewart, J.P. "Nonlinear site amplification as function of 30 m shear-wave velocity", *Earthquake Spectra*, **21**(1), pp. 1-30 (2005).
19. Day, S.M., Bielak, J., Dreger, D., Graves, R., Larsen, S., Olsen, K. and Pitarka, A., *3D Ground Motion Simulations in Basins*, PEER (2005).

20. Abrahamson, N.A. and Somerville, P.G. "Effects of the hanging wall and footwall on the ground motions recorded during the Northridge earthquake", *Bulletin of Seismological Society of America*, **86**(1), pp. 93-99 (1996).

21. Shi, B.P., Brune, J.N., Zeng, Y.H. and Anooshehpoor, A. "Dynamics of earthquake normal faulting: Two dimensional lattice particle model [J]", *Bulletin of Seismological Society of America*, **93**(3), pp. 1179-1197 (2003).

22. Chiou, B.S.J. and Youngs, R.R. "An NGA model for the average horizontal component of peak ground motion and response spectra", *Earthquake Spectra*, **24**(1), pp. 173-215 (2008).

23. Somerville, P.G. and Pitarka, A. "Differences in earthquake source and ground motion characteristics between surface and buried earthquakes", *Processing of 8th National Conference on Earthquake Engineering*, **81**(1), pp. 259-266 (2006).

24. Abrahamson, N.A. and Silva, W.J. "Summary of the Abrahamson and Silva, NGA ground-motion relations", *Earthquake Spectra*, **24**(1), pp. 67-97 (2008).

25. Ramazi, H.R. and Schenk, V. "Preliminary results obtained from strong ground motion analyses [sic] of Iranian earthquakes", *The XXIV General Assembly of the ESC*, **3**, pp. 1762-1770 (1994).

26. Zaré, M., Ghafory, A.M. and Bard, P.Y. "Attenuation law for the strong-motions in Iran", *Third International Conference on Seismology and Earthquake Engineering*, Tehran, **1**, pp. 345-354 (1999).

27. Khademi, M.H. "Attenuation of peak and spectral accelerations in the Persian plateau", *Twelfth European Conference on Earthquake Engineering*, p. 330 (2002).

28. Nowroozi, A.A. "Attenuation relations for peak horizontal and vertical accelerations of earthquake ground motion in Iran: A preliminary analysis", *Journal of Seismology and Earthquake Engineering*, **7**, pp. 109-128 (2005).

29. Mahdavian, A. "Empirical evaluation of attenuation relations of peak ground acceleration in the Zagros and central Iran", *First European Conference on Earthquake Engineering and Seismology (A Joint Event of the 13th ECEE & 30th General Assembly of the ESC)*, p. 558 (2006).

30. Zare, M. and Sabzali, S. "Spectral attenuation of strong motions in Iran", *Third International Symposium on the Effects of Surface Geology on Seismic Motion*, **1**, pp. 749-758 (2006).

31. Aghabarati, H. and Tehranizadeh, M. "Near-source attenuation relationship for the geometric mean horizontal component of peak ground acceleration and acceleration response spectra", *Asian Journal of Civil Engineering (Building and Housing)*, **9**, pp. 261-290 (2008).

32. Ghodrati, A.G. and Mahdavian, A. "Dana FM (2007b) response on the discussion of attenuation relationships for Iran", *Journal of Earthquake Engineering*, **11**(6), pp. 1036-1037.

33. Ghodrati, A.G., Khorasani, M., MirzaHessabi, M. and Razavian Amrei, S.A. "Ground-motion prediction equations of spectral ordinates and Arias intensity for Iran", *Journal of Earthquake Engineering*, **14**, pp. 1-29 (2010).

Biographies

Alireza Shokran Neam was born on April 17, 1986, and after graduation from the Department of Civil Engineering at Tabriz University in 2009, continued his studies on Earthquake Engineering at Amirkabir University of Technology and received MSc degree in 2012. His research interests are earthquake engineering, performance-based design, structural control, and structural health monitoring.

Touraj Taghikhany was born on November 13, 1969, in Tehran, Iran. After graduation from the Department of Civil Engineering at Amirkabir University of Technology in 1993, he continued his studies on Earthquake Engineering at Sharif University of Technology and received MSc degree in 1996. He was awarded a PhD in Civil Engineering and Structural Dynamics by Kyoto University, Japan, in 2004. He then joined Amirkabir University of Technology in Tehran and, presently, he is an Assistant Professor of Earthquake Engineering at this university. His current research is focused on effect of near-field ground motion on structures, earthquake-engineering performance-based probabilistic design, and application of control systems in structures.